In Situ Analysis of Single-Stranded and Duplex siRNA Integrity in Living Cells†

Koen Raemdonck, Katrien Remaut, Bart Lucas, Niek N. Sanders, Jo Demeester, and Stefaan C. De Smedt*

Laboratory of General Biochemistry and Physical Pharmacy, Faculty of Pharmaceutical Sciences, Ghent University, Harelbekestraat 72, 9000 Ghent, Belgium

Received February 20, 2006; Revised Manuscript Received July 3, 2006

ABSTRACT: To attain the full therapeutic promise of short interfering RNA (siRNA), it is believed that improvements such as increased biostability are critical. Regrettably, thus far, insufficient in situ data are on hand regarding the intracellular stability of siRNAs. We report on the use of an advanced fluorescence-based method to probe the nucleolytic decay of double labeled siRNAs, which are subject to fluorescence resonance energy transfer (FRET). In vitro measurements with RNAse A and cellular extracts demonstrate that the ratio of acceptor (5′-Cy5) to donor (3′-rhodamine green) fluorescence can be used to study the degradation of the labeled siRNA substrates upon donor excitation. Intracellular FRET analysis showed substantial degradation of single-stranded siRNA, whereas duplex siRNA stayed intact during the measured time period. These data underline the high intrinsic nuclease resistance of unmodified duplex siRNA and prove that cellular persistence is much more critical for the single-stranded structure. For the first time, the stability of siRNA is investigated in real-time inside living cells. The fluorescence-based method presented here is a straightforward technique to gain direct information on siRNA integrity inside living cells and provides a bright outlook to learn more about the intracellular fate of siRNA therapeutics.

Knockdown of gene expression by RNA interference (RNAi[1]) has evolved as a powerful tool for reverse genetic analysis and holds great therapeutic potential (*1*, *2*). RNAi represents an evolutionarily conserved gene-silencing mechanism by which ∼21 nucleotide double-stranded RNAs, termed short interfering RNAs (siRNAs) (*3*), guide the sequence-specific cleavage and subsequent degradation of the targeted mRNA and, thus, the knockdown of the corresponding gene (*4*). Intracellularly, duplex siRNA is recognized by key components of the RNAi pathway, which eventually leads to the incorporation of the antisense (guide) strand in a ribonucleoprotein complex termed RISC (RNA-induced silencing complex). This activated RISC (RISC*) subsequently degrades the target mRNA, employing the guide strand as the docking site to the homologous mRNA sequence (*1*−*5*). The discovery that siRNAs can also target mammalian genes without invoking the interferon response enlightened the path to the development of siRNA therapeutics (*5*).

To effectively use siRNAs as drug molecules, many barriers still need to be overcome (*6*). For the successful in vivo application of siRNAs, their biostability and cellular delivery should be improved (*1*, *2*, *6*−*8*). Many efforts have already been undertaken to chemically modify the siRNA molecules in order to reduce their susceptibility to RNAses (*7*, *9*−*13*). Some of the investigated modifications indeed provide a higher resistance against serum-derived nucleases (*7*, *12*, *13*). Moreover, evidence exists indicating that chemical modifications of siRNAs can lead to a prolonged gene-silencing effect in cell culture, suggesting that the transient and short-lived RNAi induced gene knockdown usually observed in mammalian cells may be partially due to intracellular siRNA degradation (*9*, *11*, *12*). However, in an attempt to confirm this hypothesis, Layzer et al. came to the conclusion that the use of nuclease-resistant siRNA does not by definition result in a more potent and/or prolonged RNAi effect in vitro and in vivo (*13*). Besides chemical modification, the packaging of siRNAs into suitable delivery carriers may also protect them from degradation, even in vivo (*8*).

The interest of numerous research groups with regard to the improvement of siRNA stability emphasizes the need for useful and straightforward methods to probe siRNA integrity. Thus far, most data on siRNA biostability are obtained from gel electrophoresis experiments following the incubation of the siRNA in serum or cellular extracts. To our knowledge, there are no reports of experiments that follow the degradation of siRNA in living cells in real-time, mainly because of the lack of suitable noninvasive methods. It is clear, however, that the development of siRNA as a drug needs an understanding of its intracellular fate. The major focus of this article is, therefore, to investigate the intracellular turnover of siRNAs. For this purpose, we assessed the enzymatic degradation of double fluorescently labeled single-stranded (ss) and double-stranded (ds) siRNA

† Koen Raemdonck is a doctoral fellow of IWT-Vlaanderen (Institute for the Promotion of Innovation through Science and Technology in Flanders). Katrien Remaut and Niek Sanders are doctoral and post-doctoral researchers, respectively, of FWO−Vlaanderen (Fund for Scientific Research-Flanders). Financial support is gratefully acknowledged.

* To whom correspondence should be addressed. Tel: 0032-9-2648076. Fax: 0032-9-2648189. E-mail: stefaan.desmedt@ugent.be.

[1] Abbreviations: siRNA, short interfering RNA; RNAi, RNA interference; mRNA, messenger RNA; RISC, RNA induced silencing complex; FRET, fluorescence resonance energy transfer; FFS, fluorescence fluctuation spectroscopy; ssRNA, single-stranded RNA; dsRNA, double-stranded RNA; RNAse, RNA degrading enzyme; F_A/F_D ratio, ratio of the acceptor (red) to donor (green) fluorescence; RhoGr, rhodamine green dye.

10.1021/bi060351b CCC: $33.50
Published on Web 08/11/2006

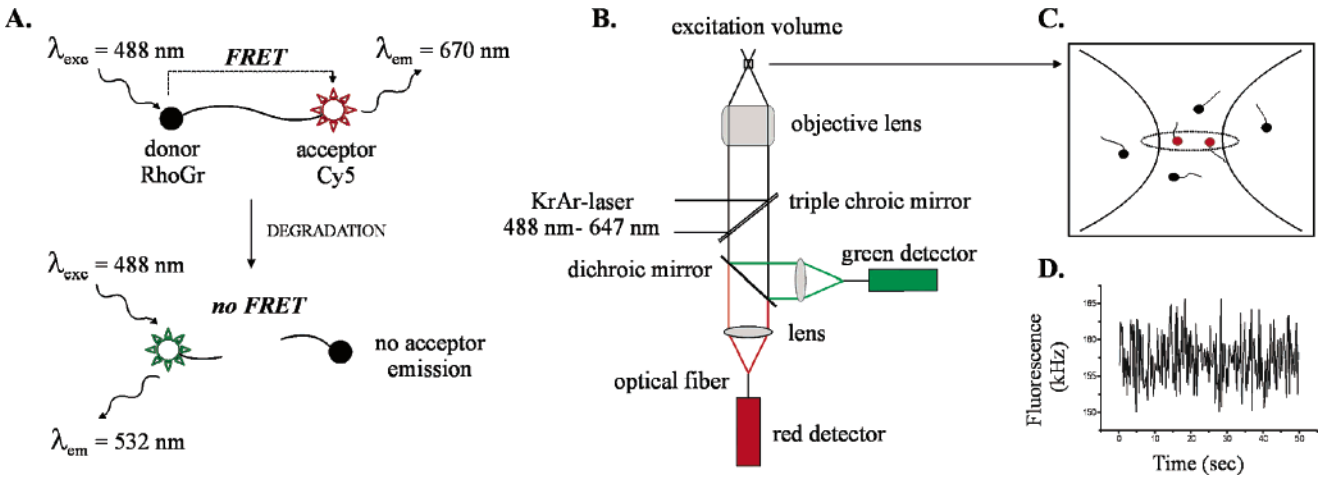

FIGURE 1: (A) Schematic representation of fluorescence resonance energy transfer (FRET) and its applicability to probe the degradation of double labeled siRNA (see Materials and Methods). (B) Setup of the dual-color fluorescence fluctuation spectroscopy (dual-color FFS) instrument. The excitation light, emerging from a Kr−Ar ion laser, is reflected by a triple chroic mirror and focused onto the objective of a confocal microscope. The fluorescence light, emitted by the fluorophores when diffusing through the excitation volume, passes the same objective and triple chroic mirror to be split by a dichroic mirror into red and green components. (C) Animated view of fluorescent molecules diffusing through the excitation volume (typically some femtoliters), which causes fluorescence intensity fluctuations as depicted in (D).

inside living cells by fluorescence resonance energy transfer (FRET; Figure 1A). The fluorescence intensities of both dyes (rhodamine green and Cy5, attached to the 3′ and 5′ ends, respectively, of the sense strand) were monitored using a dual-color fluorescence fluctuation spectroscopy setup (FFS) as depicted in Figure 1B. Essentially, FFS measures fluorescence intensity fluctuations in the excitation volume of a (confocal) microscope (Figure 1B−D). The fluorescence fluctuations are due to the movement of the fluorophores in and out the confocal volume (Figure 1C−D). In dual-color FFS, a sample containing two spectrally different fluorophores (e.g., rhodamine green and Cy5) is analyzed, and their emission light is registered separately by two detectors monitoring the *same* excitation volume (Figure 1B) (*14*).

Our results demonstrate that duplex siRNA is more resistant to intracellular nucleases than single-stranded siRNA, which is degraded within minutes. Additionally, this study shows the potential of the delineated fluorescence-based technique for future research on cell biological behavior of siRNA.

MATERIALS AND METHODS

siRNA Oligonucleotides. Twenty-one-nt single-stranded (ss) siRNAs were synthesized and purified by Eurogentec (sense strand: 5′-GUGCGCUGCUGGUGCCAACdTdT-3′; antisense strand: 5′-GUUGGCACCAGCAGCGCACdTdT-3′). Double fluorescent labeling occurred at the 3′ and 5′ ends of the sense strand with rhodamine green (RhoGr) and Cy5, respectively. The concentration of the siRNA stock solutions (in DEPC-treated water) was calculated from absorption measurements at 260 nm (1 OD_{260} = 40 μg/mL) with a Nanodrop ND-1000 spectrophotometer. The absorption of the rhodamine label at 260 nm was taken into account. The presence of the fluorescent labels was verified by absorption measurements at 500 nm for RhoGr ($\epsilon_{RhoGr,500\ nm}$ = 54 000 l·mol^{-1}·cm^{-1}) and 647 nm for Cy5 ($\epsilon_{Cy5,647\ nm}$ = 250 000 l·mol^{-1}·cm^{-1}) and revealed a 70% double labeling of the sense siRNA strand.

Fluorescent siRNA duplexes were prepared through hybridization of nonlabeled antisense and fluorescently labeled sense RNA strands (either single or double labeled). Equimolar amounts of both RNAs were mixed in an annealing buffer (final buffer concentration 50 mM Tris at pH 7.5−8.0, 100 mM NaCl), and annealing was performed in a thermal cycler (2 min incubation at 94 °C, followed by slow cooling to 25 °C over a time period of 45 min). Duplex formation was confirmed by 20% nondenaturing polyacrylamide gel electrophoresis.

Cell Culture and Microinjection Experiments. VERO cells (African green monkey kidney cells) were maintained in Dulbecco's modified eagle's medium (DMEM) without phenol red (Gibco), supplemented with 2 mM glutamine, 10% heat deactivated fetal bovine serum (FBS), and 1% penicillin-streptomycin at 37 °C in a humidified atmosphere (5% CO_2). The cells were profylactically treated against mycoplasma with Plasmocin (Invivogen). For intracellular fluorescence measurements, the cells were seeded (2.5 × 10^4 cells/cm^2) on culture dishes with a central 150 μm thick glass-bottomed surface (MatTek Corporation). The cells were incubated 24 or 48 h prior to microinjection.

Microinjection experiments were conducted with a Femtojet microinjector and an Injectman NI 2 micromanipulator (Eppendorf). All injections were performed in the cytoplasm. Directly following microinjection, intracellular fluorescence measurements were carried out as described below.

Preparation of Cytosolic and Nuclear Cell Extracts. Cytosolic and nuclear cell fractions were derived from VERO cells according to a slightly modified BD bioscience transfactor extraction protocol. Cells were harvested at high confluency by trypsinization and centrifuged at 450*g* for 5 min (4 °C). Subsequently, the cell pellets were rinsed twice by resuspension in cold phosphate buffered saline (PBS), collected again, and redispersed in a hypotonic lysis buffer (10 mM HEPES at pH 7.9, 1.5 mM $MgCl_2$, and 10 mM KCl, supplemented with Complete Mini EDTA-free Protease Inhibitor Cocktail (Roche)). Following incubation on ice (15 min) and subsequent centrifugation (5 min at 420*g*, 4 °C), the cells were again dispersed in lysis buffer equal to twice the cell pellet volume. The resulting cell suspension was slowly drawn into a narrow-gauge syringe and rapidly ejected

to disrupt the outer membrane (disruption step was repeated 10 times). Nuclei were pelleted by centrifugation of the lysed cells at 11 000*g* for 20 min. The supernatant (cytosolic extract) was collected and stored in small aliquots at −80 °C.

For preparation of the nuclear extract, the remaining nuclear pellet was resuspended in a nuclear extraction buffer (20 mM HEPES at pH 7.9, 1.5 mM $MgCl_2$, 0.42 M NaCl, 0.2 mM EDTA, 25% (v/v) glycerol), supplemented again with Complete EDTA-free Protease Inhibitor Cocktail in appropriate concentrations. Following the disruption of the nuclei (using a new syringe), the nuclear suspension was shaken gently for 30 min on ice and then centrifuged at 18 000*g* for 5 min. The supernatant (nuclear extract) was stored in small aliquots at −80 °C.

Dual-Color Fluorescence Fluctuation Spectroscopy Setup. Fluorescence measurements were performed on a dual-color FFS setup installed on a MRC1024 Bio-Rad confocal laser-scanning microscope (depicted in Figure 1B). An inverted microscope (Eclipse TE300D, Nikon) equipped with a water-immersion objective lens (Plan Apo 60×, NA 1.2, collar-rim correction, Nikon) was employed. The 488 and 647 nm laser lines of a krypton−argon laser (Bio-Rad) were used to excite the RhoGr and Cy5 dyes, respectively, and their emission signal was registered by ultrasensitive Avalanche photodiode detectors. The fluorescence intensity fluctuations were recorded on a digital ALV 5000/E correlator. The FFS setup was calibrated as described by Schwille et al. (*15*) and summarized by Remaut et al. (*16*) to optimize the overlap of the excitation and detection volumes and to determine the size of the latter.

A detailed outline of the theoretical concept and applications of FFS can be found elsewhere (*17*, *18*). In this study, the dual-color FFS setup is mainly employed to measure the fluorescence intensities of labeled siRNA present at nanomolar concentrations. Additional correlation analysis of the fluorescence fluctuations to obtain information on the mobility of the siRNA molecules was not performed. Therefore, the mathematical basics and diffusion models to be applied to the FFS data will not be covered in this article.

siRNA Stability Analysis. Fluorescence resonance energy transfer (FRET) is an important research tool to study inter and intramolecular processes and is defined as the nonradiative excitation energy transfer from a donor fluorophore to an appropriate acceptor fluorophore when both dyes are fixed in close proximity (typically ∼10−100 Å) (*19*). The energy transfer efficiency is inversely proportional to the sixth power of the interdye distance (*19*). Hence, virtually any process that induces distance variations between a donor and an acceptor on the nanometer scale can be monitored with this technique (*20*). In this article, FRET is used as a tool to study the degradation of double-labeled siRNAs (see Results). Intact nucleic acid molecules, baring both a donor and acceptor, show a significant acceptor emission upon donor excitation due to energy transfer, as schematically illustrated in Figure 1A. When the double-labeled substrates are cleaved into single-labeled products, FRET can no longer occur, resulting in negligible acceptor fluorescence. Basically, the ratio of the 5′-Cy5 fluorescence (acceptor fluorophore) to the 3′-RhoGr fluorescence (donor fluorophore) upon donor excitation (termed F_A/F_D) correlates with siRNA integrity (see Results). For the determination of the F_A/F_D ratio on degrading siRNAs, the fluorescence intensities of RhoGr and Cy5 were recorded for 3 s by the green and red detectors, respectively (Figure 1B), with laser excitation set at 488 nm. All samples were analyzed in glass-bottomed 96-well plates (Greiner Bio-One, certified DNAse/RNAse free), and the focal volume was placed 50 μm above the bottom of the wells.

Degradation experiments with RNAse A (RPA grade, manufactured from bovine pancreas, Ambion) were performed at ambient temperature by first diluting the siRNA stock solutions with RNAse A buffer (100 mM Tris-acetate at pH 6.5, 1 mM EDTA, 1 mM cyclic 2′,3′-cytidine monophosphate) to a final concentration of 13 nM. Subsequently, 1 μL of RNAse A solution was added, and F_A/F_D was measured as a function of time.

To monitor the degradation of siRNAs in cytosolic and nuclear extracts of VERO cells, a siRNA solution (400 nM) in degradation buffer (20 mM Tris-HCl, 50 mM Na-acetate, 2 mM Mg-acetate, adjusted with sodium hydroxide to pH 7.4) was mixed with 50% (v/v) of cellular extract and incubated at 37 °C in nonstick RNAse free microfuge tubes (Ambion). Aliquots were taken at different time points and diluted with sodium citrate buffer to stop degradation (for *dsRNA* degradation: 10 mM sodium citrate at pH 4, 0.025% sodium dodecylsulfate (SDS); for *ssRNA* degradation: 10 mM sodium citrate at pH 6, 20 mM DTT, 0.1% SDS). Samples (end concentration 13 nM) were analyzed immediately or incubated on ice prior to F_A/F_D measurements.

To monitor the stability of siRNA in VERO cells, first, confocal images were taken of the cells, and the FFS observation volume was positioned inside the nucleus. Solutions of intact ssRNA (10 μM), intact dsRNA (6 μM), (RNAse A) degraded ssRNA (10 μM), and (RNAse A) degraded dsRNA (6 μM) were prepared in RNAse-free water and loaded into a microinjection needle (Eppendorf II). Subsequently, cells were microinjected into the cytoplasm. Approximately 30 to 60 s after the injection, the cells were exposed to 488 nm laser light, and the F_A/F_D ratio was determined in the nucleus. The low laser excitation power and the short measurement time ensured minimal photobleaching and cellular damage. For the time-dependent stability analysis, the F_A/F_D ratio was registered inside the nucleus at different time-points after injection. At the end of each data series, we verified that the nucleus was still in focus.

Polyacrylamide Gel Electrophoresis Combined with Dual-Color FFS. siRNA duplex (8 μM) (27.5 μL) was added to 0.48 μg of RNAse A in 12.5 μL of RNAse A buffer without cyclic 2′,3′-cytidine monophosphate and incubated at room temperature. At specified times, 5 μL (for gel electrophoresis, ∼ 0.4 μg of siRNA) and 0.5 μL aliquots (for dual-color FFS) were removed. Electrophoresis aliquots were mixed with 10 μL of formamide (with 0.05% bromophenol blue), snap frozen at −80 °C and stored afterward at −20 °C. A 20% polyacrylamide gel, supplemented with 7 M ureum in TBE buffer (0.089 M Tris base, 0.089 M boric acid (pH 8.35), 2 mM Na_2EDTA), was applied to analyze siRNA degradation (40 min run at 100V). Following electrophoresis, the gel was stained (40 min) in a $1:10^4$ dilution of SYBR Green II RNA stain (Molecular Probes) in DEPC-treated water, and samples were visualized on a UV Trans-illuminator. The 0.5 μL aliquots were added to 7 μL of RNAse A buffer and also

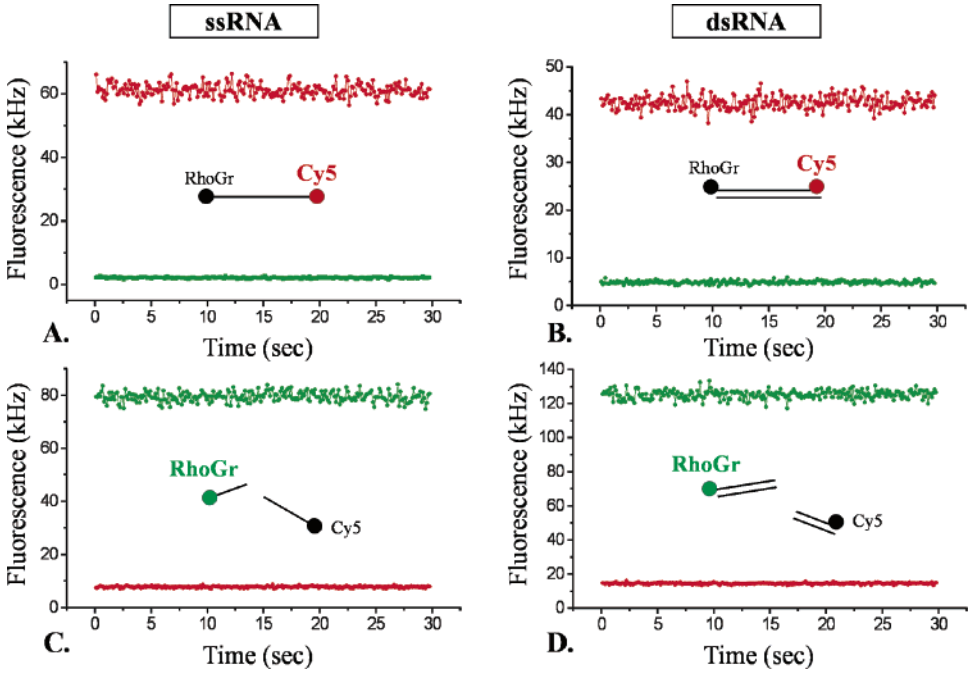

FIGURE 2: Fluorescence fluctuation profiles of intact/degraded ssRNA (A and C) and dsRNA (B and D) obtained in DEPC-treated water upon 488 nm excitation. A graphical representation of the predominant siRNA species in the measured samples is added. Intact siRNA shows a higher Cy5 fluorescence signal compared to that of RhoGr because of fluorescence resonance energy transfer (FRET). When the oligos are degraded, FRET can no longer occur, eventually leading to the inversion of the emission profile.

snap frozen at −80 °C. The F_A/F_D ratio (upon 488 nm excitation) of every aliquot was calculated.

RESULTS

FRET as a Tool to Distinguish between Intact and Degraded Single-Stranded and Duplex siRNA. Figure 2 shows representative fluorescence fluctuation profiles obtained for intact ssRNA (Figure 2A) and intact dsRNA (Figure 2B) in DEPC-treated water upon 488 nm excitation. Although only rhodamine green (RhoGr) can be efficiently excited with these settings, the Cy5 fluorescence (red signal) markedly exceeds the RhoGr fluorescence (green signal). This clearly indicates that energy from the RhoGr excited state (donor) is transferred to and excites the Cy5 acceptor dye (FRET). The ratio of acceptor fluorescence to donor fluorescence upon 488 nm excitation (F_A/F_D ratio) is used here as a measure for energy transfer (see Materials and Methods). Table 1 summarizes the F_A/F_D values measured for ssRNA and dsRNA. Both intact ssRNA and dsRNA display a F_A/F_D ratio $\gg 1$ in DEPC-treated water, which is mainly due to FRET. Upon annealing with nonlabeled complementary siRNA, the F_A/F_D ratio of ssRNA clearly lowers, indicating that the energy transfer is partially inhibited in the duplex form. This is probably explained by a higher rigidity of the duplex structure, which makes the relative position of both dyes less optimal for FRET. Also, the F_A/F_D value seems to depend on the medium in which siRNA is diluted (Table 1). When siRNA is placed in RNAse A buffer or sodium citrate buffer, a lower F_A/F_D ratio was measured in comparison with F_A/F_D in DEPC-treated water (Table 1), indicating that in the buffer media energy transfer is significantly diminished.

Fluorescence fluctuations (upon 488 nm excitation) of degraded siRNA samples are shown in Figure 2C and D. In contrast with the fluorescence fluctuation profiles of intact siRNA samples, now, the RhoGr emission becomes dominant. This red-to-green shift is due to the degradation of the siRNAs, which separates donor and acceptor dyes, thus precluding energy transfer (Figure 1A). siRNA degradation is also clearly reflected in the F_A/F_D values (Table 1). Incubation of siRNA in the presence of RNAse A and cellular extracts (derived from VERO cells) no longer allows FRET and significantly lowers the F_A/F_D ratio ($F_A/F_D \ll 1$).

To further unravel the F_A/F_D turnover during degradation, the red and green fluorescence were monitored in time after the addition of RNAse A. In this experiment, an excess of RNAse A was added to allow for the monitoring of a significant decrease in F_A/F_D on a short time-scale (400 s) with continuous laser excitation. As can be seen in Figure 3A, the degradation of ssRNA corresponds to an increase in

Table 1: Overview of the Measured F_A/F_D Ratios of Single-Stranded (ss) and Double-Stranded (ds) siRNA[a]

intact	in DEPC-treated water	in buffer A	in buffer B
ssRNA	29.3 ± 2.0	15.5 ± 2.1	19.6 ± 1.9
dsRNA	9.5 ± 0.8	1.5 ± 0.1	1.9 ± 0.1
degraded	**RNAse A**	**nuclear extract**	**cytoplasmic extract**
ssRNA	0.11 ± 0.01	0.13 ± 0.01	0.12 ± 0.01
dsRNA	0.11 ± 0.00	0.09 ± 0.01	0.14 ± 0.01

[a] Intact siRNA oligos show a high ratio primarily due to FRET. Degradation of siRNA in the presence of cellular extracts or RNAse A corresponds to $F_A/F_D \ll 1$. Ratios were calculated on the basis of average red and green fluorescence intensities, measured over a 30 s time frame (excitation wavelength equaled 488 nm). Different samples were analyzed, and F_A/F_D ratios are presented as mean values ± standard deviation of at least three independent experiments. Buffer A: RNAse A buffer; buffer B: sodium citrate buffer, supplemented with SDS.

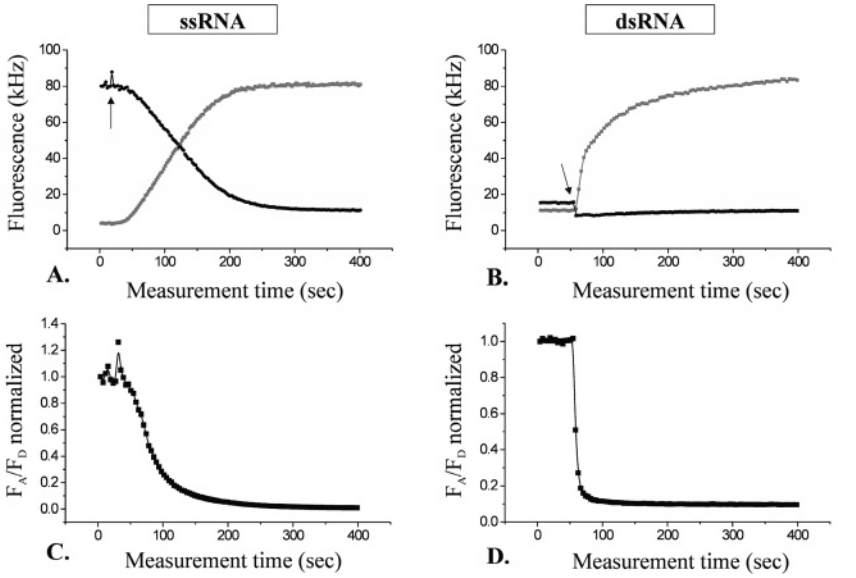

FIGURE 3: (A and B) Real-time emission behavior of double fluorescently labeled siRNAs (488 nm excitation). The analysis was performed through continuous excitation over a 400 s time-interval of a 13 nM siRNA solution (in RNAse A buffer) incubated at ambient temperature together with an excess of RNAse A (2.5 ng and 1.5 μg of RNAse A for ssRNA and dsRNA, respectively). Arrows indicate the time-point of RNAse A addition. Degradation of ssRNA results in an increase in RhoGr emission (gray data) and a concomitant decrease in Cy5 fluorescence (black data) because of the disappearance of FRET. Regarding the siRNA duplex, the F_A/F_D ratio is primarily influenced by the increase in donor fluorescence. (C and D) Time-dependent profiles of the resulting F_A/F_D ratio. To normalize the results, the F_A/F_D ratio of intact siRNA was set to 1.

green fluorescence and a concomitant decrease in red fluorescence because of the disappearance of FRET. During degradation of dsRNA, green fluorescence also gradually increases, whereas red fluorescence remains almost unchanged (Figure 3B). We observed that the degradation of *single* RhoGr labeled siRNAs also increases the green fluorescence, which we attributed to RhoGr dequenching (data not shown). That this phenomenon also occurs in double labeled siRNAs cannot be excluded. In other words, one can say that the change in F_A/F_D upon degradation of ssRNA and dsRNA is governed by both a loss of FRET and intramolecular RhoGr fluorescence dequenching. It is important to emphasize that a direct comparison of ssRNA and dsRNA degradation kinetics cannot be made from F_A/F_D measurements because of the fact that different processes influence the decrease in F_A/F_D ratio of ssRNA and dsRNA. More importantly however, Figure 3 parts C and D clearly illustrate that the F_A/F_D ratio can be used to follow the conversion between intact and degraded siRNA.

Monitoring the Degradation of ssRNA and dsRNA in RNAse A Solutions. First, we tried to characterize the correlation between the F_A/F_D ratio and the percentage of degraded siRNA in a sample. Hereto, different amounts of intact and degraded siRNA (resulting from long-term incubation at 37 °C with nuclear or cytosolic extract) were mixed and the F_A/F_D ratio was determined. As can be seen in Figure 4, a higher amount of degraded siRNA corresponds with a lower F_A/F_D ratio, although a linear relation was not found. When the sample contains only degraded siRNA, the F_A/F_D value drops to ca. 0.6% and 5% of its initial value for respectively ssRNA (Figure 4A) and dsRNA (Figure 4B).

Figure 5 shows the degradation profiles of ssRNA and dsRNA after addition of different amounts of RNAse A. Breakdown of the RNA initially strongly lowers the F_A/F_D ratio followed by a more gradual decrease. As expected, adding higher amounts of enzyme results in a faster decrease

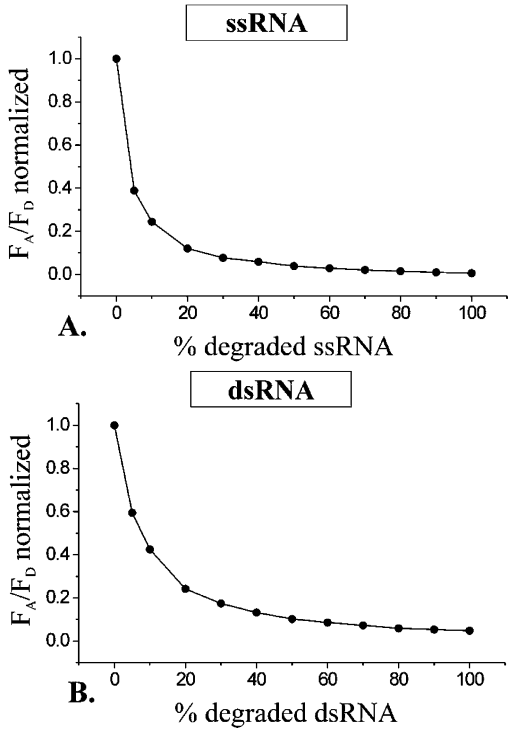

FIGURE 4: Correlation between the F_A/F_D ratio and the percentage of degraded siRNA in a mixture of intact and degraded siRNA (in sodium citrate buffer, supplemented with SDS). The F_A/F_D ratio decreases with increasing concentrations of degraded siRNA because only intact RNA can contribute to the FRET signal. The F_A/F_D ratio of intact RNA was normalized to a value of 1.

in the F_A/F_D ratio, which reflects a higher degradation rate. RNAse A is an endonuclease with a single-strand substrate specificity that cleaves 3′ from C and U residues. Only low amounts of RNAse A are needed to degrade a nanomolar ssRNA sample (Figure 5A). However, at higher enzyme concentrations also dsRNA is subject to degradation (Figure

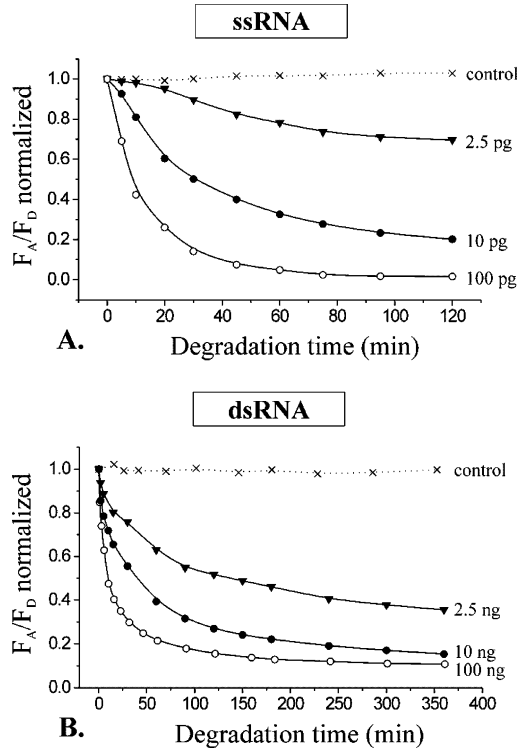

FIGURE 5: (A and B) Time-dependent degradation profiles (normalized F_A/F_D as a function of degradation time) of ssRNA and dsRNA with different amounts of RNAse A (depicted in both parts) in RNAse buffer. The siRNA concentration was equal in all samples (13 nM). FFS measurements were performed at ambient temperature with laser excitation set at 488 nm. Control measurements were in RNAse buffer alone.

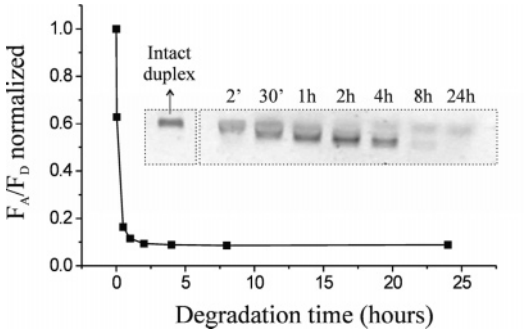

FIGURE 6: Gel electrophoresis on degrading dsRNA samples. RNAse A (0.48 μg) was added to a 5.5 μM dsRNA solution in RNAse A buffer without cyclic 2′-3′-cytidine monophosphate. At different incubation times (ambient temperature), FFS aliquots were taken and snap frozen at −80 °C. Prior to measurement, the samples were diluted to a concentration suitable for FFS analysis**.** The normalized F_A/F_D ratio as a function of degradation time is shown. Electrophoresis aliquots (~0.4 μg of dsRNA) were taken at the same time points and also stored immediately at −80 °C. Graph insert shows the corresponding dsRNA degradation profile visualized with SYBR Green II RNA stain on a denaturing 20% polyacrylamide gel.

5B). Indeed, it is known that the specificity of RNAse A is dependent on the concentration used.

To visualize dsRNA degradation we performed denaturing PAGE gel electrophoresis (Figure 6, graph insert). As expected, a clear degradation pattern could be seen. After 24 h of incubation almost no detectable nucleic acid fragments were remaining on the gel. FFS based stability analysis on the degrading samples was performed in parallel (Figure 6) and elucidated that merely mixing the dsRNA with

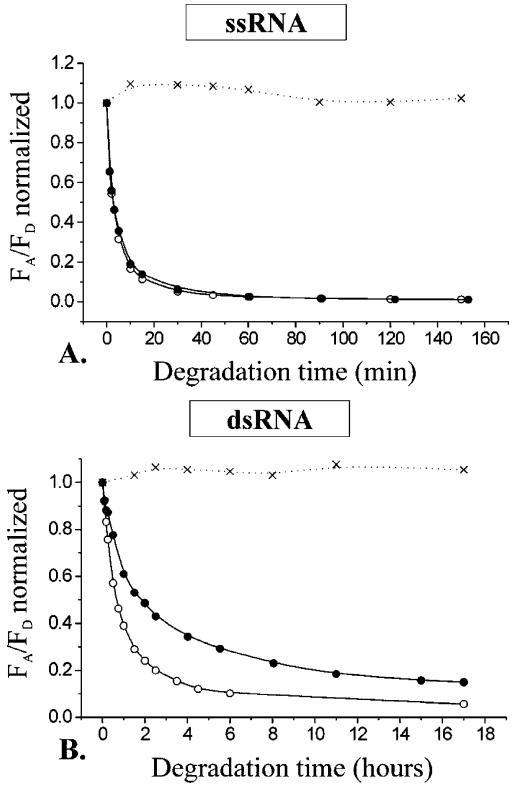

FIGURE 7: FFS measurements performed on degrading siRNA oligos in cellular extracts. Crude extracts were mixed with twice the volume of a 400 nM RNA solution in degradation buffer and incubated at 37 °C. At different time points, an aliquot was mixed with SDS−sodium citrate buffer to a final concentration of 13 nM. Excitation wavelength equaled 488 nm, and fluorescence intensities were recorded during 3 s. F_A/F_D ratios were again normalized to a value of 1. No difference in degradation rate could be observed for ssRNA in pure cytoplasmic (●) and nuclear extracts (○). Concerning dsRNA however, the F_A/F_D ratio shows a faster decay in the nuclear extract compared to that in the cytosolic extract. Blank measurements (×) were performed in degradation buffer alone (dsRNA) or degradation buffer supplemented with 0.1% SDS (ssRNA). The influence of siRNA−protein binding on the measured F_A/F_D signal was minimized through dilution of the samples in the denaturing buffer prior to measurement.

RNAse (corresponding with the 2′ time point) already reduced the F_A/F_D ratio by 37%. Following 2 h of incubation the F_A/F_D ratio does not decrease any further. This indicates that the degradation primarily takes place during the first 2 h of incubation. As almost no full length fragments remained visible on the gel at the 2 h time point, the information obtained from respectively the gel electrophoresis measurements and the F_A/F_D measurements are in well agreement, indicating that the F_A/F_D ratio effectively reflects the amount of intact and/or degraded double labeled siRNA in a sample.

Monitoring the Degradation of ssRNA and dsRNA in Cellular Extracts. In the next step, we wondered whether the FRET-FFS technique also allows the study of the stability of siRNA in more complex media. Hereto, cytoplasmic and nuclear fractions were isolated from VERO cells and incubated with single- and double-stranded RNA. Figure 7 shows the corresponding degradation profiles. The first interesting observation is that single-stranded RNA is almost completely degraded after 60 min of incubation (Figure 7A), whereas complete degradation of duplex siRNA, even after several hours of incubation, was not obtained (Figure 7B). A significantly slower degradation rate was seen when

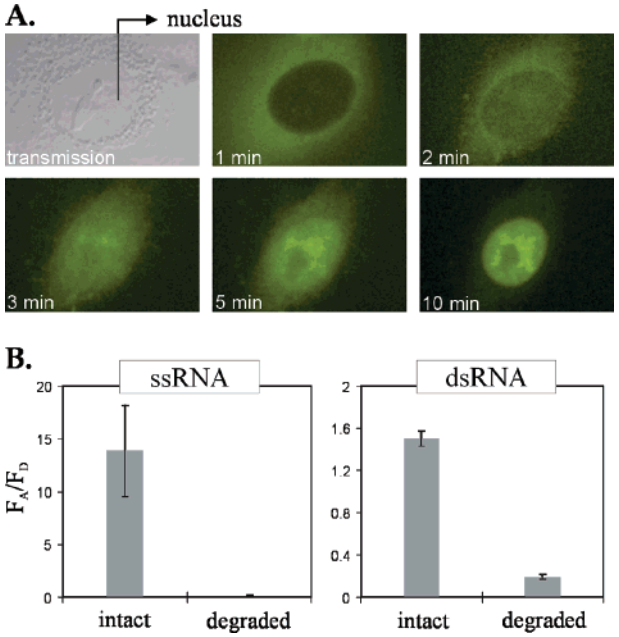

FIGURE 8: (A) Transmission image and confocal images (488 nm excitation) of VERO cells taken at different time points after cytoplasmic injection of dsRNA. (B) F_A/F_D ratio measured in cells after microinjecting intact or (previously) degraded ssRNA and dsRNA. The FFS observation volume was positioned in the nucleus of the injected cell with laser excitation set at 488 nm. The F_A/F_D ratio is presented as the mean value ± standard deviation obtained from at least three independent experiments under identical calibration.

experiments were repeated with 1/10 diluted extract (data not shown). Surprisingly, ssRNA seems to degrade equally fast in cytoplasmic extract as in nuclear extract (Figure 7A), indicating that both extracts possess a comparable ssRNAse activity. However, regarding the siRNA duplex, the F_A/F_D ratio shows a considerably faster decay in nuclear extract compared to that in cytosolic extract. This observation suggests that, under given assay conditions, much higher dsRNAse activity was present in the nuclear fraction of the VERO cells.

Monitoring the Intracellular Degradation of ssRNA and dsRNA. Having established that the F_A/F_D ratio is a reliable parameter to follow siRNA integrity in cellular extracts, we next aimed to analyze the intracellular stability of siRNA in living cells using microinjection to deliver the siRNA to the cytosol. Figure 8A shows confocal images (488 nm excitation) of VERO cells taken at different time points after cytoplasmic injection of a high concentration of intact dsRNA. Duplex siRNA seems to rapidly accumulate in the nucleus after injection and clearly does not show a homogeneous intranuclear distribution. A comparable behavior has already been observed for antisense oligonucleotides (*21*). Also, single-stranded siRNA showed a fast nuclear accumulation (data not shown). Hence, further exploration of the intracellular integrity of both siRNAs was performed in the nucleus of the injected VERO cells. Figure 8B depicts the F_A/F_D ratio measured in the nuclei directly after microinjecting intact or previously degraded (ss and ds, respectively) siRNA in the cytosol of the cells. Because the FFS setup makes use of much more sensitive detectors than a conventional fluorescence microscope, a lower amount of siRNA was injected here. For injected intact siRNA, a F_A/F_D ratio >1 was calculated, whereas F_A/F_D remained far below 1 when degraded siRNA was introduced in the cytosol. This clearly demonstrates that the dual-color FFS setup can distinguish between intact and degraded siRNA inside living cells.

Next, we aimed to characterize the intracellular degradation rate of duplex siRNA in VERO cells. For this purpose, we microinjected intact double-stranded siRNA in the cytosol of VERO cells and positioned the FFS observation volume in the nucleus of the cell. During the first half hour following injection of dsRNA, an increase in both the red and green nuclear fluorescence was observed (Figure 9A), in agreement with the nuclear accumulation of duplex siRNA as seen in Figure 8A. Subsequently, a slow decay in the fluorescence intensities was observed, which can be attributed to a redistribution of intact nuclear dsRNA to the cytosolic compartment. A similar behavior was reported for antisense oligonucleotides, which seem to shuttle between the nucleus and cytoplasm (*22*). Interestingly, the F_A/F_D ratio remains constant over the measured time interval (Figure 9C), demonstrating that the duplex siRNA stays intact. This is in contrast to the degradation of dsRNA in cellular extracts, as concluded from Figure 7B. These observations prove that siRNA stability in cellular extracts cannot just be translated to the actual cellular environment and highlight that in situ measurements are needed.

Intracellular measurements with ssRNA revealed a vast lowering of the F_A/F_D ratio (Figure 9D), indicating the disappearance of FRET and RhoGr quenching and, thus, ssRNA degradation. The intracellular data emphasize the high stability of duplex siRNA and the high instability of single-stranded siRNA, in line with other reports in the literature (*10*, *11*). Interestingly, in Figure 9B, again a concomitant increase in red and green fluorescence was registered in the nucleus during the first 5 min, attributed to the nuclear import of the ssRNA. Clearly, the single-stranded siRNA shows a faster accumulation than duplex siRNA. However, the relative increase in red fluorescence is less pronounced than the increase in green fluorescence, explaining the F_A/F_D decline within this time frame. It can be postulated that upon injecting ssRNA in the cytoplasm, a fraction of the RNA will be readily degraded. Hence, during the first few minutes after microinjection, a mix of degraded and intact ssRNA is prone to nuclear import. It goes without saying that the intact single-stranded siRNA molecules that reach the nucleus will also degrade within a reasonable time span. As outlined previously, ssRNA degradation results in an increase in green fluorescence and a parallel lowering of the red fluorescence. Because the red emission already drops at 5 min after injection (Figure 9B), we conclude that some intact siRNAs still reach the nucleus but that the siRNA molecules at this moment are subject to intranuclear degradation. One can wonder why the green fluorescence in the nucleus remains more or less constant between 5 and 50 min following injection. Probably, the loss of intranuclear fluorescence due to nucleocytoplasmic redistribution of (intact and already degraded) siRNA is countered by the increase in green fluorescence as a result of degradation. Approximately 60 min after injection, the F_A/F_D no longer drops (Figure 9D), indicating that no further degradation occurs. The slight decrease in red and green fluorescence is now completely attributed to diffusion of siRNA fragments from the nucleus into the cytoplasm.

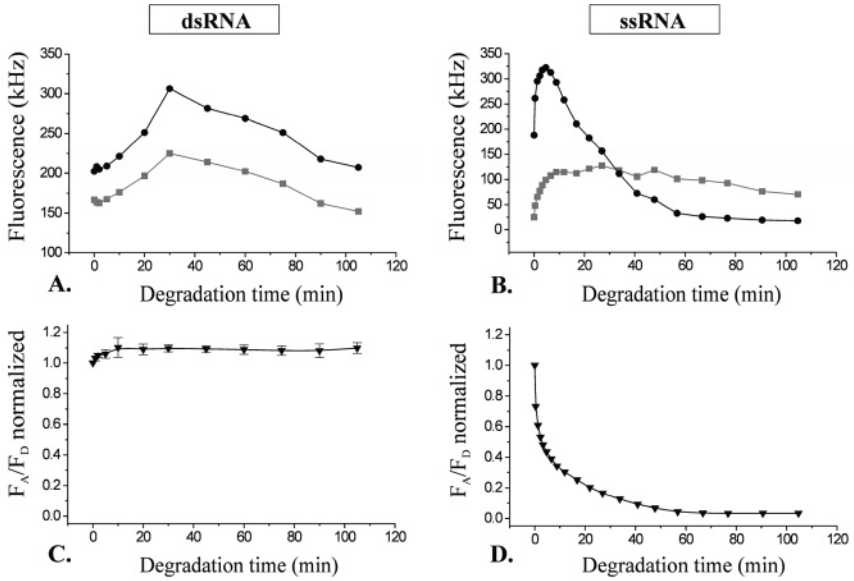

FIGURE 9: Intranuclear fluorescence intensity profile of (A) dsRNA and (B) ssRNA. The emission signal in both the green (■, gray) and red (●, black) detector is shown as a function of degradation time. (C and D) Corresponding time-dependent degradation profiles of dsRNA and ssRNA obtained in the nucleus of VERO cells. Laser excitation was set at 488 nm and microinjection was conducted in the cytoplasm of the focus cell. Normalized F_A/F_D ratios of dsRNA are presented as mean values ± standard deviation of three independent experiments under different calibration. ssRNA data are from one representative of three independent experiments.

DISCUSSION

Many disease-causing genes can be silenced efficiently in cell culture with rationally designed short interfering RNAs under optimized transfection conditions. However, the application of siRNA therapeutics is not yet conceivable because siRNA delivery, biodistribution, target cell selectivity, and so forth remain major hurdles to be overtaken. Obviously, the therapeutic success of siRNA will also greatly depend on the biostability of siRNA. Indeed, the siRNA molecules should be sufficiently stable in the extra and intracellular matrixes to be able to exert a biological effect (*1*, *2*, *6*).

Previous reports in the literature have studied the degradation of synthetic RNA/DNA chimera (*23*) and antisense oligonucleotides by FRET (ref 14 (*14*) and refs therein). Also inside living cells, FRET has been used to evaluate ribozyme cleavage of a labeled oligoribonucleotide substrate (*24*) and detect intact and degraded oligonucleotides (*14*, *25*). In the present study, we first wanted to evaluate whether the dual-color FFS setup (as depicted in Figure 1B) is suited to probe the nucleolytic decay of double fluorescently labeled siRNAs that are subject to FRET. Figures 3−7 clearly show that the F_A/F_D ratio obtained from the fluorescence fluctuation data (measured through the FFS setup) can be applied to study the transition from intact to degraded siRNA. As single-stranded siRNA shows much higher FRET efficiency than duplex siRNA (Table 1), this also allows us to distinguish between dsRNA degradation and duplex strand denaturation. Although dsRNA degradation results in a decrease in the F_A/F_D ratio, destabilization of the intact siRNA duplex will eventually lead to an increase in the F_A/F_D ratio. Indeed, the release of the more flexible siRNA sense strand from the duplex structure will induce a higher FRET signal.

Correlation analysis on the fluorescence fluctuation profiles will allow the calculation of the diffusion coefficient of the fluorescently tagged molecules passing through the observation volume of the confocal microscope (*15*, *17*, *18*). However, this strategy is not recommended for monitoring the degradation of siRNA as a function of time (*16*). Strictly, FFS can only distinguish between fluorescent molecules with sufficiently different mobility, that is, when their diffusion coefficients (D) differ by at least a factor of 1.6 (*26*). Considering that $D \approx 1/(\mathrm{MW})^{1/3}$, this implies that FFS could only differentiate between intact and *fully* degraded siRNA. In contrast, FRET is sensitive to a single cleavage, irrespective of the molecular weight (MW) of the degradation products formed (*16*). It is also worth highlighting that in this article end-labeled siRNAs are used. It could be argued that the labels sterically interfere with (primarily) exoribonuclease binding to the siRNA substrate, thereby limiting the enzymatic activity, which would then lead to an underestimation of the degradation rate.

Using a confocal FFS setup to register the fluorescence intensities is particularly advantageous for quantifying the intracellular fate of siRNAs. Indeed, the confocal excitation volume can be easily placed inside a defined cellular compartment. As the fluorescence photons emanating from this focal spot are registered by ultrasensitive photodiode detectors, this enables us to measure nanomolar concentrations of fluorescent molecules, which are often too low for FRET when studied through confocal imaging. For future siRNA research, this could be especially attractive because only low concentrations of highly active siRNA are needed to show a biological effect. It is also known that fluorescence from endogenous cellular components (autofluorescence) may interfere with FFS measurements in mammalian cells, especially when excitation wavelengths in the blue spectral range (<500 nm) are used (*27*). In particular, the autofluorescence signal may render the interpretation of intracellular data challenging (*28*), especially when the fluorescently labeled molecules of interest are present at low concentration. In this article, the intracellular fluorescence exceeded the autofluorescence at least 5-fold at every data point, ensuring

that the obtained F_A/F_D ratios really reflect the fate of the injected siRNAs.

Confocal images showed nuclear accumulation of dsRNA when microinjected in the cytoplasm (Figure 8A). Several reports, however, present evidence for the cytoplasmic nature of RNAi as activated RISC complexes that localize and function in the cytosol where translation of target mRNA takes place (*29*). Transfection of Hela cells with TAT_{47-57}−siRNA conjugates, siRNA/lipofectamine nanoparticles, or siRNA/polyamidoamine nanoparticles revealed that the siRNAs preferentially locate in the perinuclear region, thought to contain focal points of RNAi machinery (*30*). This specific subcellular localization showed strong correlation with RNAi activity (*30*). A recent article, however, declared that RNAi activity is also present in the nucleus of HeLa cells because functional RISC complexes were found in both nuclear and cytoplasmic extracts (*31*). Thus, upon transfection, short interfering RNA that is released from its carrier presumably enters the nucleus and forms RISC* complexes on site to cleave homologous nuclear RNA transcripts. It has also been shown in the literature that siRNAs can induce transcriptional gene silencing in mammalian cells through DNA methylation, a process that occurs in the nucleus (*32*). The confocal images presented in Figure 8 also show a distinct intranuclear accumulation pattern around the nucleolus that in itself remains largely unlabeled. This could potentially indicate the presence of nuclear binding sites or siRNA complexes. The observed intranuclear distribution contradicts the findings of Ohrt et al. (*33*), who found that microinjected siRNAs are excluded from the nucleoplasm by a RanGTP/Exportine 5 pathway but not from the nucleolus. Apparently, many uncertainties on the intracellular fate of siRNA do remain and emphasize the need for advanced methods to investigate them. However, one should keep in mind that the intracellular distribution of siRNAs will probably depend on how they are delivered to the cytosol.

Intracellular FFS measurements showed substantial degradation of the single-stranded RNA. In contrast, the F_A/F_D ratio measured for dsRNA remained unchanged for almost 2 h, emphasizing the high intrinsic stability of dsRNA (Figure 9C). Probably, the low dsRNAse activity in both the cytoplasmic and nuclear compartment compared to the higher load of single-strand specific nucleases accounts for the discrepancy in the stability of ssRNA and dsRNA. A recent article on the stability of native siRNAs in serum revealed that duplex siRNA is mainly degraded by enzymes of the (ss)RNAse A family (*34*). Some of these enzymes can be termed single-strand *preferring* because they are also capable of degrading double-stranded RNA, although to a much lesser extent. The biochemical mechanism of this process has already been described in the literature (*35*). Inside a living cell, there are numerous types of ribonucleases (exo and endoribonucleases) with different structures and catalytic function (*36*). Because of the high complexity and diversity of this class of molecules, it is difficult to predict the predominant ribonuclease pathway involved in the intracellular degradation of siRNA.

Because only one siRNA sequence was studied in this article, it is not possible to draw any conclusions with regard to the sequence-dependent degradation of siRNA. However, on the basis of the fact that different articles suggest that single-stranded siRNA degrades faster than a siRNA duplex (*3*, *10*, *11*, *43*), we are quite confident that in general for native siRNAs the duplex structure will show a higher stability in a biological environment compared to the stability of the single-stranded counterpart.

The observations in Figure 9 also raise an interesting question of how RISC incorporation of the double-labeled siRNA duplex would influence the observed F_A/F_D profile. The assembly of the (unlabeled) guide strand into RISC, followed by the unwinding of the duplex structure and release of the (double labeled) passenger strand would imply degradation of the latter (*37*, *38*). As a consequence, single labeled RNA fragments would diffuse into the nucleus and cause a decrease in the F_A/F_D ratio, which is not observed here. Because blocking of the 5′-end of the antisense strand can abolish RNAi activity and a free terminal 5′-phosphate is believed to be essential for RNAi activity (*33*, *39*−*42*), it is very unlikely that the 3′-5′ double labeled siRNA strand will act as the guide strand. From this, we eventually conclude that RISC activation does not occur under these experimental conditions. It is possible that relatively high intracellular siRNA concentrations lead to the saturation of the cellular compartments and the RNAi machinery, thereby masking the interaction of siRNA with RISC. Although some explanations exist for this observation, the how and why remains largely unclear.

It could be hypothesized that the lower stability of ssRNA is partially responsible for the less effective gene silencing activity of antisense siRNA compared to that of duplex siRNA (*3*, *43*). It has been suggested that single-stranded antisense siRNA can also directly enter the mammalian RNAi pathway with subsequent depletion of endogenous gene expression (*9*, *42*, *43*), but still, the duplex siRNA potency generally exceeds the single-stranded RNAi activity. Also, in most cases, duplex siRNA shows a more persistent gene silencing than antisense DNA oligonucleotides (*1*, *2*, *12*), which is, according to Bertrand et al. (*44*), primarily attributed to their difference in susceptibility for nuclease attack.

The stability data we present here have been gathered inside living cells after microinjection of the siRNA molecules in the cytosol. Because no transfection procedure was applied, the intracellular environment to which the microinjected siRNAs are exposed resembles that of siRNAs released from a pharmaceutical nanocarrier (e.g., liposomes and polymeric nanoparticles) into the cytoplasm. Because the applied delivery system, together with incorporation of the antisense siRNA strand into RISC, could provide extra protection of the siRNA against nuclease attack, the time frame especially between release from its carrier and interaction with RISC will be crucial for siRNA integrity inside the intracellular matrix (*43*). Our results suggest that intracellular degradation is much more critical for ssRNA than for duplex siRNA. The observation that modified siRNA duplexes with enhanced nuclease resistance do not always show longer lasting RNAi effect (*13*) supports our hypothesis that intracellular stability is not the key issue for effective application of siRNA duplexes. It can be postulated that upon delivery to the cytosol, nonmodified duplex siRNA is able to induce a response before significant degradation occurs (*13*). Hence, further research into functional in vivo delivery systems that can safely guide active siRNA to the cytosol of the target cell should be stimulated.

ACKNOWLEDGMENT

We thank critical readers for valuable comments on the manuscript. We are grateful to N. Opitz (Max Planck Institute for Molecular Physiology, Dortmund, Germany) for installing the FFS-module on the MRC1024.

REFERENCES

1. Dorsett, Y., and Tuschl, T. (2004) siRNAs: Applications in functional genomics and potential as therapeutics, *Nat. Rev. Drug Discovery 3*, 318−329.
2. Dykxhoorn, D. M., and Lieberman, J. (2005) The silent revolution: RNA interference as basic biology, research tool and therapeutic, *Annu. Rev. Med. 56*, 401−423.
3. Elbashir, S. M., Lendeckel, W., and Tuschl, T. (2001) RNA interference is mediated by 21-and 22-nucleotide RNAs, *Genes Dev. 15*, 188−200.
4. Zamore, P. D., Tuschl, T., Sharp, P. A., and Bartel, D. P. (2000) RNAi: Double-stranded RNA directs the ATP-dependent cleavage of mRNA at 21 to 23 nucleotide intervals, *Cell 101*, 25−33.
5. Elbashir, S. M., Harborth, J., Lendeckel, W., Yalcin, A., Weber, K., and Tuschl, T. (2001) Duplexes of 21-nucleotide RNAs mediate RNA interference in cultured mammalian cells, *Nature 411*, 494−498.
6. Schiffelers, R. M., Woodle, M. C., and Puthupparampil, S. (2004) Pharmaceutical prospects for RNA interference, *Pharm. Res. 21*, 1−7.
7. Elmen, J., Thonberg, H., Ljungberg, K., Frieden, M., Westergaard, M., Xu, Y., Wahren, B., Liang, Z., Ørum, H., Koch, T., and Wahlestedt, C. (2005) Locked nucleic acid (LNA) mediated improvements in siRNA stability and functionality, *Nucleic Acids Res. 33*, 439−447.
8. Urban-Klein, B., Werth, S., Abuharbeid, S., Czubayko, F., and Aigner, A. (2005) RNAi-mediated gene-targeting through systemic application of polyethylenimine (PEI)-complexed siRNA in vivo, *Gene Ther. 12*, 461−466.
9. Amarzguioui, M., Holen, T., Babaie, E., and Prydz, H. (2003) Tolerance for mutations and chemical modifications in a siRNA, *Nucleic Acids Res. 31*, 589−595.
10. Braasch, D. A., Jensen, S., Liu, Y., Kaur, K., Arar, K., White, M. A., and Corey, D. R. (2003) RNA interference in mammalian cells by chemically-modified RNA, *Biochemistry 42*, 7967−7975.
11. Chiu, Y.-L., and Rana, T. M. (2003) siRNA function in RNAi: A chemical modification analysis, *RNA 9*, 1034−1048.
12. Czauderna, F., Fechtner, M., Dames, S., Aygün, H., Klippel, A., Pronk, G. J., Giese, K., and Kaufmann, J. (2003) Structural variations and stabilising modifications of synthetic siRNAs in mammalian cells, *Nucleic Acids Res. 31*, 2705−2716.
13. Layzer, J. M., McCaffrey, A. P., Tanner, A. K., Huang, Z., Kay, M. A., and Sullenger, B. A. (2004) In vivo activity of nuclease-resistant siRNAs, *RNA 10*, 766−771.
14. De Smedt, S. C., Remaut, K., Lucas, B., Braeckmans, K., Sanders, N. N., Demeester, J. (2005) Studying biophysical barriers to DNA delivery by advanced light microscopy, *Adv. Drug Delivery Rev. 57*, 191−210.
15. Schwille, P., Meyer-Almes, F., Rigler, R. (1997) Dual-color fluorescence cross-correlation spectroscopy for multicomponent diffusional analysis in solution, *Biophys. J. 72*, 1878−1886.
16. Remaut, K., Lucas, B., Braeckmans, K., Sanders, N. N., De Smedt, S. C., Demeester, J. (2005) FRET-FCS as a tool to evaluate the stability of oligonucleotide drugs after intracellular delivery, *J. Controlled Release 103*, 259−271.
17. Elson, E. S., Magde, D. (1974) Fluorescence correlation spectroscopy: I. Conceptual basis and theory, *Biopolymers 13*, 1−27.
18. *Fluorescence Correlation Spectroscopy: Theory and Applications* (2001) (Rigler, R., and Elson, E. L., Eds.) Springer-Verlag, Berlin-Heidelberg, Germany.
19. Clegg, R. M. (1992) Fluorescence resonance energy transfer and nucleic acids, *Methods Enzymol. 211*, 353−389.
20. Selvin, P. R. (2000) The renaissance of fluorescence resonance energy transfer, *Nat. Struct. Biol. 7*, 730−734.
21. Leonetti, J. P., Mechti, N., Degols, G., Gagnor, C., and Lebleu, B. (1991) Intracellular distribution of microinjected antisense oligonucleotides, *Proc. Natl Acad. Sci. U.S.A. 88*, 2702−2706.
22. Lorenz, P., Misteli, T., Baker, B. F., Bennett, C. F., and Spector, D. L. (2000) Nucleocytoplasmic shuttling: a novel *in vivo* property of antisense phosphorothioate oligodeoxynucleotides, *Nucleic Acids Res. 28*, 582−592.
23. Uhler, S. A., Cai, D., Man, Y., Figge, C., and Walter, N. G. (2003) RNA degradation in cell extracts: Real-time monitoring by fluorescence resonance energy transfer, *J. Am. Chem. Soc. 125*, 14230−14231.
24. Vitiello, D., Pecchia, D. B., and Burke, J. M. (2000) Intracellular ribozyme-catalyzed *trans*-cleavage of RNA monitored by fluorescence resonance energy transfer, *RNA 6*, 628−637.
25. Uchiyama, H., Hirano, K., Kashiwasake-Jibu, M., and Taira, K. (1996) Detection of undegraded oligonucleotides *in vivo* by fluorescence resonance energy transfer, *J. Biol. Chem. 271*, 380−384.
26. Meseth, U., Wohland, T., Rigler, R., and Vogel, H. (1999) Resolution of fluorescence correlation measurements, *Biophys. J. 76*, 1619−1631.
27. Schwille, P. (2001) Fluorescence correlation spectroscopy and its potential for intracellular applications, *Cell. Biochem. Biophys. 34*, 383−408.
28. Brock, R., Hink, M. A., and Jovin, T. M. (1998) Fluorescence correlation microscopy of cells in the presence of autofluorescence, *Biophys. J. 75*, 2547−2557.
29. Zeng, Y., and Cullen, B. R. (2002) RNA interference in human cells is restricted to the cytoplasm, *RNA 8*, 855−860.
30. Chiu, Y.-L., Ali, A., Chu, C.-Y., Cao, H., and Rana, T. M. (2004) Visualizing a correlation between siRNA localization, cellular uptake, and RNAi in living cells, *Chem. Biol. 11*, 1165−1175.
31. Robb, G. B., Brown, K. M., Khurana, J., and Rana, T. M. (2005) Specific and potent RNAi in the nucleus of human cells, *Nat. Struct. Mol. Biol. 12*, 133−137.
32. Matzke, M. A., and Birchler, J. A. (2005) RNAi-mediated pathways in the nucleus, *Nat. Rev. Genet. 6*, 24−35.
33. Ohrt, T., Merkle, D., Birkenfeld, K., Echeverri, C. J., and Schwille, P. (2006) In situ fluorescence analysis demonstrates active siRNA exclusion from the nucleus by Exportin 5, *Nucleic Acids Res. 34*, 1369−1380.
34. Haupenthal, J., Baehr, C., Kiermayer, S., Zeuzem, S., and Piiper, A. (2006) Inhibition of RNAse A family enzymes prevents degradation and loss of silencing activity of siRNAs in serum, *Biochem. Pharmacol. 71*, 702−710.
35. Sorrentino, S., Naddeo, M., Russo, A., and D'Alessio, G. (2003) Degradation of double-stranded RNA by human pancreatic ribonuclease: Crucial role of noncatalytic basic amino acid residues, *Biochemistry 42*, 10182−10190.
36. Deutscher, M. P., and Li, Z. W. (2001) Exoribonucleases and their multiple roles in RNA metabolism, *Prog. Nucleic Acid Res. Mol. Biol. 66*, 67−105.
37. Leuschner, P. J. F., Ameres, S. L., Kueng, S., and Martinez, J. (2006) Cleavage of the siRNA passenger strand during RISC assembly in human cells, *EMBO Rep. 7*, 314−320.
38. Schwarz, D. S., Hutvagner, G., Du, T., Xu, Z., Aronin, N., and Zamore, P. D. (2003) Asymmetry in the assembly of the RNAi enzyme complex, *Cell 115*, 199−208.
39. Nykanen, A., Haley, B., and Zamore, P. D. (2001) ATP requirements and small interfering RNA structure in the RNA interference pathway, *Cell 107*, 309−321.
40. Harborth, J., Elbashir, S. M., Vandenburgh, K., Manninga, H., Scaringe, S. A., Weber, K., and Tuschl, T. (2003) Sequence, chemical, and structural variation of small interfering RNAs and short hairpin RNAs and the effect on mammalian gene silencing, *Antisense Nucleic Acid Drug Dev. 13*, 83−105.
41. Chiu, Y.-L., and Rana, T. M. (2002) RNAi in human cells: basic structural and functional features of small interfering RNA, *Mol. Cell 10*, 549−561.
42. Martinez, J., Patkaniowska, A., Urlaub, H., Lührmann, R., and Tuschl, T. (2002) Single-stranded antisense siRNAs guide target RNA cleavage in RNAi, *Cell 110*, 563−574.
43. Holen, T., Amarzguioui, M., Babaie, E., and Prydz, H. (2003) Similar behavior of single-strand and double-strand siRNAs suggests they act through a common RNAi pathway, *Nucleic Acids Res. 31*, 2401−2407.
44. Bertrand, J.-R., Pottier, M., Vekris, A., Opolon, P., Maksimenko, A., and Malvy, C. (2002) Comparison of antisense oligonucleotides and siRNAs in cell culture and in vivo, *Biochem. Biophys. Res. Commun. 296*, 1000−1004.

BI060351B